# 9

# Multicriteria Analysis of $\mathcal{L}_1$ Adaptive Flight Control System

## 9.1 Objective of the Research

Inner-loop adaptive flight control systems[1] are seen as an appealing technology [1] to improve aircraft performance with reduced pilot compensation in adverse flight conditions or in the event of control surface failures and vehicle damage. Under these conditions, which are characterized by a high degree of uncertainty with respect to a nominal aircraft model, the achievable levels of performance and flying qualities (FQ) that a nonadaptive flight control system (FCS) can provide might be limited. However, in applications with stringent performance and robustness specifications [2], several limitations of conventional adaptive control architectures have been identified that render the design of these conventional adaptive controllers overly challenging. Among these limitations [2, 3], are of special relevance: (1) the lack of transient characterization of the closed-loop response, (2) the limited analysis framework for robustness and performance guarantees for closed-loop adaptive systems, and (3) the lack of systematic design guidelines to solve the trade-off between adaptation, performance, and robustness.

 The $\mathcal{L}_1$ adaptive control theory [4] appeared recently as a method for the design of robust adaptive control architectures using fast estimation schemes, with the potential to overcome the limitations mentioned above. The key feature of $\mathcal{L}_1$ adaptive control is the decoupling of adaptation and robustness. In fact, in $\mathcal{L}_1$ adaptive control architectures, the speed of adaptation is limited

---

1. Chapter 9 is written in collaboration with Enrick Xargay and Vladimir Dobrokhodov.

only by the available hardware (computational power and high-frequency sensor noise), while the trade-off between performance and robustness can be addressed via conventional methods from classical and robust control. Fast adaptation, which allows for the compensation of the undesirable effects of rapidly varying uncertainties and significant changes in system dynamics, is critical towards achieving guaranteed transient performance without enforcing persistency of excitation, applying gain scheduling of the control parameters, or resorting to control reconfiguration or high-gain feedback. Moreover, the systematic design procedures of the $\mathfrak{L}_1$ adaptive control theory significantly reduce the tuning effort required to achieve a desired closed-loop performance, which translates into a reduction in both the design cycle time and the development costs. With these features, the $\mathfrak{L}_1$ adaptive control architectures provide a suitable framework for the development of advanced flight critical systems.

In this chapter, we present the preliminary results of the application of the PSI method for the design optimization of the $\mathfrak{L}_1$ flight control system implemented on the GTM AirSTAR [5, 6] aircraft's current primary flight test vehicle, the GTM tail number T2. The T2 is a twin-engine jet-powered and dynamically-scaled (5.5%) civil transport aircraft, designed and instrumented to perform control law evaluation, experiment design and modeling research, in-flight failure emulation, and flight in upset conditions. The research control law developed for the NASA AirSTAR flight test vehicle has a primary objective of achieving tracking for a variety of tasks with guaranteed stability and robustness in the presence of uncertain dynamics, such as changes due to rapidly varying flight conditions during standard maneuvers, and unexpected failures. Ideally, the flight control system should provide level 1 flying qualities under nominal as well as adverse flight conditions.

The $\mathfrak{L}_1$ flight control system ($\mathfrak{L}_1$ FCS) used for this application is a three-axis angle of attack ($\alpha$), roll rate ($p$), and sideslip angle ($\beta$) all-adaptive flight control system. The FCS consists of two decoupled $\mathfrak{L}_1$ controllers, one for the longitudinal channel and another one for the control of the lateral-directional dynamics. On the one hand, the longitudinal $\mathfrak{L}_1$ controller is implemented as a single-input single-output controller and uses feedback in angle of attack and pitch rate to generate an elevator control signal in order to track angle of attack reference signals; on the other hand, the lateral/directional $\mathfrak{L}_1$ controller is a multiple-input multiple-output architecture and uses feedback in sideslip angle, roll rate, and yaw rate to generate aileron and rudder commands in order to track sideslip-angle and roll-rate reference signals with reduced coupling. In the current $\mathfrak{L}_1$ FCS, the pilot directly adjusts the thrust level using the throttle lever. The reader is referred to [7–9] for a more detailed explanation of the $\mathfrak{L}_1$ FCS implemented on the NASA AirSTAR flight test vehicle.

The main challenge for the design of the $\mathfrak{L}_1$ FCS is the optimal tuning of its elements to provide desired flying qualities with satisfactory robustness

margins. While the theory of $\mathcal{L}_1$ adaptive control provides partial systematic design guidelines to address the trade-off between performance and robustness, the optimization of the design of the $\mathcal{L}_1$ adaptive controller is still largely open and hard to address. The main difficulty is the nonconvex and nonsmooth nature of the underlying optimization problem that involves the $\mathcal{L}_1$ norm of cascaded linear systems. Randomized algorithms have been proven to be useful in control-related nonconvex optimization problems, and therefore they appear as appealing methods for the optimal design of $\mathcal{L}_1$ adaptive controllers [4, 10].

The optimization design methodology proposed in this chapter unfolds in three sequential steps. First, we take advantage of the systematic design guidelines of the $\mathcal{L}_1$ adaptive control theory to find a nominal prototype solution satisfying a given set of control specifications. Then, taking the prototype solution as a reference design, the PSI method is used for the construction of the feasible solution set and for determining an initial direction of improvement for the design of the flight control system [11–13]. Finally, the PSI method is again used to determine an optimal design that satisfies performance and robustness constraints and improves the prototype design. In particular, this design methodology demonstrates the suitability of the PSI method as a tool for formulating and solving multicriteria optimization problems for the design of adaptive FCS and also illustrates that the consistent application of the systematic design guidelines of $\mathcal{L}_1$ adaptive control becomes particularly beneficial for the construction of the feasible solution set.

Following this approach, we next present preliminary results on the application of the PSI method and the MOVI software [12] to the design optimization of the $\mathcal{L}_1$ FCS for the NASA GTM. We notice that, although both the PSI and the software package MOVI were specially developed to address problems with design variable and the criteria spaces of high dimensionality, for the sake of clarity in the presentation and discussion of the results, we keep the design problem within a reasonable complexity, and the design procedure is applied to the design of the longitudinal channel only. Finally, we also notice that the results included in this study are obtained by the MOVI software package combined with the MATLAB environment and are based on the full nonlinear simulation of the two-engine-powered, dynamically-scaled GTM AirSTAR system tail number T2, which was released by NASA in December 2009 [14].

The formulation of the design optimization of the $\mathcal{L}_1$ FCS of the NASA AirSTAR flight test vehicle is addressed in Section 9.2. In particular, this section provides a detailed discussion of the workflow of the optimization process, including the identification of a nominal prototype design, the construction of the feasible solution set, and the improvement of the prototype. Finally, Section 9.3 provides solution of the optimization problem and summarizes the key results and presents the main conclusions.

## 9.2 Prototype: Criteria and Design Variables

The design of the longitudinal $\mathfrak{L}_1$ FCS is based on the linearized short-period dynamics of the GTM at the reference flight condition (80 kt, 1,000 ft). The $\mathfrak{L}_1$ FCS with its main elements and the design variables (DV) is represented in Figure 9.1 with a following corresponding explanation of the control architecture. The motivated choice of the DVs will be given in the following section. Since the airplane is level 1 FQ at this flight condition[2], the desired dynamics of the state predictor are chosen to be close to those of the actual aircraft.

For the nominal prototype design, the natural frequency of the poles of the system is reduced from $6\frac{rad}{sec}$ to $5.5\frac{rad}{sec}$, while the damping ratio is increased from 0.47 to 0.85. A first-order lowpass filter with DC gain 1 and a bandwidth of $20\frac{rad}{sec}$ was used in the matched contribution to the elevator command, while two cascaded first-order lowpass filters were used in the unmatched channel, both having DC gain equal to 1 and bandwidths of $5\frac{rad}{sec}$ and $7\frac{rad}{sec}$, respectively. Finally, the adaptation sampling time was set to $\frac{1}{600}$, which corresponds to the minimum integration step allowed in the AirSTAR flight control computer. A first-order prefilter with $20\frac{rad}{sec}$ of bandwidth was added to shape the pilot command. This prototype design of the state predictor, the lowpass filters, the adaptation sampling rate, and the prefilter delivers the angle of attack $\alpha$ (AOA) response similar to the desired one; see Figure 9.2 where $\alpha_{des}$ designates the desired angle-of-attack response.

It is worth noting here that this nominal design ensures a time-delay margin of the inner loop of approximately 85 ms and a gain margin of 7.2 dB, in wings-level flight at the flight condition of 80 knots and 1,000 ft. At this flight condition, the FQs are predicted to be level 1 and the FCS design has no predicted pilot induced oscillation (PIO) tendencies (for an acquisition time of 1.5 seconds). Naturally, these metrics are the performance criteria, and their initial values provided above for the nominal design will serve as the guidelines for the motivated definition of the criteria constraints.

We next present preliminary results of the application of the PSI method and the MOVI software to the design optimization of the $\mathfrak{L}_1$ FCS for the NASA GTM airplane [11–13]. In particular, the objective of the optimization task is to minimize the difference between the desired and actual AOA responses, while ensuring satisfactory FQs and not overloading the elevator actuators. For

2. This FQ rating is based on offset-landing tasks performed in the AirSTAR real-time simulator at NASA LARC in the absence of atmospheric turbulence.

this purpose, a number of criteria reflecting the differences were formulated. The corresponding discussion is presented in the following sections.

For the sake of clarity in the presentation and discussion of the results, we keep the design problem within a reasonable complexity, and the design procedure is applied to the design of the longitudinal channel only. In what follows, we provide a description of the design variables alone with the performance and robustness metrics used for this study and obtain a prototype design that achieves desired flying qualities with satisfactory robustness margins. Then we utilize the capability of the PSI method and the software package MOVI to improve the prototype design.

### 9.2.1  Design Variables

Next we define the set of design parameters of the flight control architecture considered for optimization. Since the primary objective is to improve the flying qualities of the prototype design while guaranteeing satisfactory robustness margins, we include the natural frequency and the damping ratio of the poles of the state-predictor dynamics (which can speed up or slow down the response of the augmented aircraft), and the bandwidth of the lowpass filter in the matched channel (which can be used to adjust the time-delay margin of the inner loop) as optimization parameters; see Figure 9.1 illustrating their place in the $\mathcal{L}_1$ flight control architecture. In addition, we also consider the optimization of the bandwidth of the prefilter, which can be used to shape the pilot command as to prevent elevator rate limiting and avoid structural mode-flight interaction.
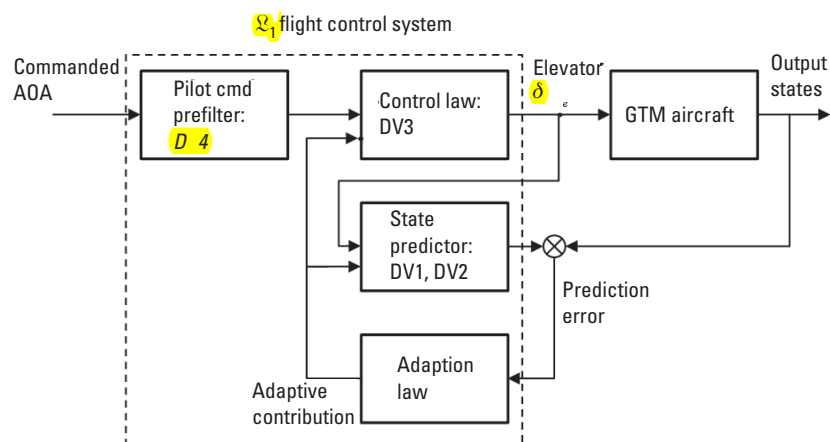


**Figure 9.1**  Longitudinal channel of the $\mathcal{L}_1$ flight control architecture.

The following list summarizes the set of optimization parameters that define the design variable space:

- *DV1:* Natural frequency of the state-predictor poles (rad/sec);
- *DV2:* Damping ratio of the state-predictor poles;
- *DV3:* Bandwidth of the "matched" lowpass filter (rad/sec);
- *DV4:* Bandwidth of the pilot-command prefilter (rad/sec).

Therefore, the design variable vector is *DV* = {*DV1, DV2, DV3, DV4*}. We notice that, consistent with the theory of $\mathcal{L}_1$ adaptive control, the adaptation sampling time is set to match the minimum integration step allowed in the AirSTAR flight control computer, and therefore it is not included as an optimization parameter.

### 9.2.2   List of Criteria and Pseudo-Criteria

The set of design criteria considered in this study is chosen to evaluate performance and robustness properties of the GTM aircraft augmented with the $\mathcal{L}_1$ FCS. To provide an adequate assessment of the performance characteristics and flying qualities of the $\mathcal{L}_1$-augmented aircraft both pilot-off-the-loop and pilot-in-the-loop performance metrics are included in the design procedure. The metrics considered can thus be classified in three categories:

1. Pilot-off-the-loop performance metrics;
2. Robustness metrics;
3. Flying qualities and PIO metrics.

Because the present material addresses only the design of the longitudinal channel of the $\mathcal{L}_1$ FCS, the set of metrics used in this study are mainly based on the (time-domain) longitudinal response of the GTM with the $\mathcal{L}_1$ FCS closing the inner loop. Furthermore, we provide a detailed description of the specific metrics used for the design improvement of the adaptive control system. We note that some of the metrics used in this study were also proposed in [15] for the evaluation of aircraft augmented with an adaptive FCS.

#### 9.2.2.1   Pilot-off-the-Loop Performance Metrics

This first set of metrics evaluates the pilot-off-the-loop performance of the augmented aircraft by characterizing its response to step inputs. In particular, the pilot-off-the-loop performance metrics are based on the time-domain response of the augmented aircraft to a step command of 3° held for 4 seconds in the AOA (see Figure 9.2), starting from a wings-level flight condition. The metrics

capture the deviation of the actual response of the aircraft from a given desired response, which is defined to provide satisfactory flying qualities without reaching the physical limits of the platform, as well as different measures of control activity, load factor, and cross-coupling.

Next we provide a description of the metrics included in the study. First, however, we need to introduce some key notation to facilitate the definition of these metrics. Below, alone with the previously defined $\alpha$ (AOA) and $\alpha_{des}$, the $\alpha_{cmd}$ is the angle-of-attack pilot command; $\beta$ is the angle of sideslip; $\beta_{des}$ is the sideslip-angle desired response; $p$ is the roll rate; $p_{des}$ is the roll-rate desired response; $A_z$ is the vertical acceleration; $\delta_e$ is the elevator deflection command; and $\tilde{x}(t)$ is the $\mathcal{L}_1$ state predictor error.

Let $t_0$ be the time instant at which the step command is applied, and define $t_f$ as the final time instant considered for the performance evaluation ($t_f = t_0 + 4$ seconds). With these notations, the metrics are defined as follows:

- *P1, final deviation:* This metric captures the final deviation of the actual AOA response from the desired AOA response at 4 seconds after the application of the step command. This metric is set to zero if the actual response reaches the AOA reference command before the end of the 4-second step:

$$P1 = \left\{ \begin{array}{l} \left| \alpha\left(t_f\right) - \alpha_{des}\left(t_f\right) \right| \ \text{if} \ \alpha\left(f\right) < \alpha_{cmd}, \forall t \in \left[t_0, t_f\right] \\ 0 \hspace{7.5cm} \text{otherwise} \end{array} \right\}$$

This metric can be used to penalize or exclude sluggish responses. In this study this metric is normalized to the amplitude of the step command (3°).
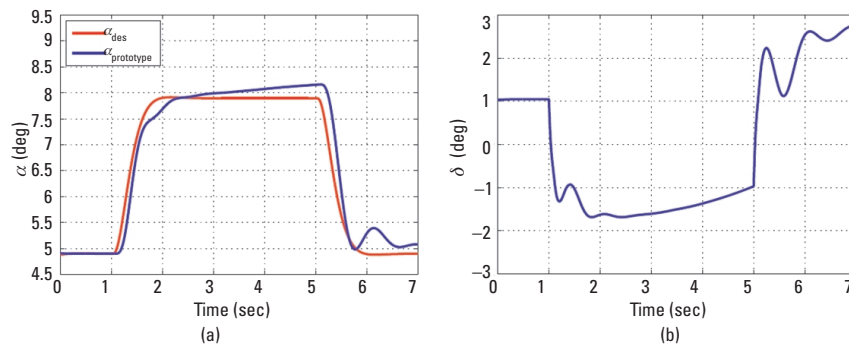


**Figure 9.2** Prototype design, 3°-AOA step response for the prototype design.

- *P2, maximum deviation from desired AOA response:* This metric captures the maximum deviation (in absolute value) of the actual AOA response from the desired AOA response:

$$P2 = \max_{t \in [t_0, t_f]} |\alpha(t) - \alpha_{des}(t)|$$

This metric can be redefined in terms of normalized AOA responses.

- *P3. Integral deviation from desired AOA response:* This metric is defined as the (truncated) $\mathcal{L}_2$ norm of the deviation of the actual AOA response from the desired AOA response:

$$P3 = \int_{t_0}^{t_f} |\alpha(t) - \alpha_{des}(t)| \, dt$$

Similar to P2, this metric can be redefined in terms of normalized AOA responses.

- *P4, overshoot in AOA response:* This metric captures possible overshoots and low-damping characteristics in the AOA response:

$$P4 = \begin{cases} \max_{t \in [t_0, t_f]} |\alpha(t)| \text{ if } \alpha(t) > \alpha_{cmd}, \text{for some } t \in [t_0, t_f] \\ \alpha_{cmd} \qquad\qquad\qquad \text{otherwise} \end{cases}$$

Similar to P1, this metric can be normalized to the amplitude of the step command (3°).

- *P5, maximum deviation from desired AOA rate response:* This metric captures the maximum rate deviation (in absolute value) of the actual AOA response from the desired AOA response:

$$P5 = \max_{t \in [t_0, t_f]} |\dot{\alpha}(t) - \dot{\alpha}_{des}(t)|$$

Similar to P2 and P3, this metric can be redefined in terms of normalized AOA responses.

- P6, integral deviation from desired AOA rate response: This metric is defined as the (truncated) $\mathcal{L}_2$ norm of the rate deviation of the actual AOA response from the desired AOA response:

$$P6 = \int_{t_0}^{t_f} \left| \dot{\alpha}(t) - \dot{\alpha}_{des}(t) \right| dt$$

Similar to P2, P3, and P5, this metric can be redefined in terms of normalized AOA responses.

The metrics P1 to P6 provide a good first characterization of the transient response of the augmented aircraft when compared to a given desired response. Next, we present a set of metrics that can be extracted from the same step response experiment utilizing different flight dynamics characteristics which complement the AOA-based metrics defined above.

- P7, maximum vertical acceleration: Load factor (and passenger comfort) requirements can be captured by the maximum vertical acceleration during the step response:

$$P7 = \max_{t \in [t_0, t_f]} \left| A_z(t) \right|$$

  This metric can also be normalized to the amplitude of the step command (3°).

- P8, control effort: This metric is defined as the (truncated) $\mathcal{L}_2$ norm of the elevator deflection command:

$$P8 = \int_{t_0}^{t_f} \left| \delta_e(t) \right| dt$$

  Similar to P1, P4, and P7, this metric can be normalized to the amplitude of the step command (3°). This metric can be used to penalize flight control designs that require a high control activity to achieve a desired control objective. It is important to note, however, that a high control effort might just be the result of a faster AOA response, and therefore a large P8 might not always be an undesirable response characteristic.

- P9, maximum elevator rate: Excessive control rate can be identified by the following metric:

$$P9 = \max_{t \in [t_0, t_f]} \left| \dot{\delta}_e(t) \right|$$

This metric, which can also be normalized to the amplitude of the step command (3°), can be used to penalize designs with high elevator rates in order to prevent undesirable effects from rate limiting.

- {blist}P10, maximum elevator acceleration: High-order derivatives of the control commands are coupled to the flexible modes of the aircraft. The following metric, based on the second derivative of the elevator command, can be used to capture excessive accelerations and oscillations in the control command that could potentially lead to unwanted structural mode interactions:

$$P10 = \max_{t \in [t_0, t_f]} \left| \ddot{\delta}_e(t) \right|$$

This metric can also be normalized to the amplitude of the step command (3°).

- P11, maximum of $\mathfrak{L}_1$ prediction error: This metric captures the maximum error between the actual system state and the state of the $\mathfrak{L}_1$ state predictor, usually denoted by $\tilde{x}(t)$:

$$P11 = \max_{t \in [t_0, t_f]} \left\| \tilde{x}(t) \right\|_\infty$$

In $\mathfrak{L}_1$ adaptive control architectures, the accurate estimation of system uncertainties and the performance guarantees rely on the (small) "size" of the prediction error $\tilde{x}(t)$. This metric can thus be used to monitor the correct functioning of the $\mathfrak{L}_1$ adaptive controller.

- P12, maximum deviation in cross-coupling dynamics: This metric captures the lateral-directional coupling induced by a command in the longitudinal channel:

$$P12 = \max_{t \in [t_0, t_f]} \left| \delta_e(t) \right| \left( \left( \beta(t) - \beta_{des}(t) \right)^2 + \left( p(t) - p_{des}(t) \right)^2 \right)$$

We notice that this metric, which can also be normalized to the amplitude of the step command (3°), provides valuable information for the design of the lateral-directional FCS, rather than the longitudinal FCS. In fact, for the design of the longitudinal $\mathfrak{L}_1$ FCS, this metric provides little information and it would be more convenient to analyze the coupling in the AOA response induced by a command either in roll rate or sideslip angle. The analysis of the response of the system to commands in the lateral-directional channel and the design of the lateral-directional $\mathfrak{L}_1$ FCS are left (deliberately) for future work.

- P13, integral deviation in cross-coupling dynamics: This metric is the integral version of the previous cross-coupling metric and is defined as follows:

$$P13 = \int_{t_0}^{t_f} \left|\delta_e(t)\right| \left(\left(\beta(t) - \beta_{des}(t)\right)^2 + \left(p(t) - p_{des}(t)\right)^2\right) dt$$

Similar to P12, this metric would be more adequate for the design of the lateral-directional control system, and it is included in this study only to illustrate a set of additional metrics that can be derived from the response of the augmented aircraft to a command in the longitudinal channel.

### 9.2.2.2 Robustness Margins

In this preliminary study, the only robustness metric considered for optimization is the time-delay margin of the closed-loop adaptive system defined at the input of the aircraft (time delay inserted at the elevator deflection command), and it is also derived from the time-domain response of the augmented aircraft. For a given wings-level flight condition and with the pilot off the loop, a small perturbation in the trim (initial) condition is introduced. The time-delay margin is determined as the minimum time delay that produces sustained oscillations in the AOA response as the $\mathcal{L}_1$ FCS tries to stabilize the aircraft at the given trim condition. In this chapter, this robustness metric will be denoted by R1.

We notice that the time delay introduced in the elevator control channel is in addition to any time delay that is already modeled in the AirSTAR simulation environment, which amounts approximately to 25 ms.

### 9.2.3 Criteria Addressing FQ and PIO Characteristics

Finally, predictions for both flying qualities and PIO tendencies have also been included in order to complement the pilot-off-the-loop performance metrics presented above. For this study, we consider the time-domain Neal-Smith (TDNS) flying qualities and PIO criteria, which were specifically developed for nonlinear aircraft dynamics and nonlinear FCS. The TDNS criterion is the counterpart in the time domain of the frequency-domain Neal-Smith criterion, and it is based on a step-tracking task with different acquisition-time requirements. For a detailed description of this criterion, the reader is referred to [16]. The reader can also find in [17] a study on the prediction of flying qualities and adverse pilot interactions in the GTM augmented with the $\mathcal{L}_1$ {**AU: Edit OK?**} FCS.

We use four different metrics, extracting all of them from the TDNS criterion for an acquisition time of 1.5 seconds, to characterize the FQ and PIO tendencies of the augmented aircraft:

- FQ1, tracking performance: In the TDNS criterion, the root-mean-squared tracking error is used to evaluate the closed-loop performance with the pilot in the loop. A value of zero means that the pilot is able to perfectly track (with zero error) the reference command after the specified acquisition time.

- FQ2, pilot workload: In the TDNS criterion, the pilot workload is given by the pilot compensation phase angle (in degrees), which is derived from the optimal pilot model obtained from the criterion. A value of zero means that there is no need for either pilot lead compensation or lag compensation.

- FQ3, FQ level: The two metrics FQ1 and FQ2 are used to determine the predicted FQ level based on the FQ boundaries proposed in the criterion. FQ3 is a discrete metric, and it only admits the values 1, 2, and 3, which correspond to level 1, level 2, and level 3 flying qualities, respectively.

- FQ4, PIO tendency: The TDNS criterion also provides a prediction for the susceptibility of the augmented aircraft to PIO. This PIO-susceptibility metric is used to complement the flying qualities metrics discussed above. According to the TDNS criterion, a value above 100 implies that the augmented aircraft is PIO-prone, whereas a value below 100 indicates a PIO-immune configuration.

The set of FQ metrics is used at the second step when improving a prototype design of the longitudinal channel of the $\mathfrak{L}_1$ FCS. For the first step of the prototype design and the exploration of the feasible set, only a subset of these metrics is utilized. The full set of metrics is used in the last stage to optimize the design of the adaptive control system.

Based on the objectives of the task and previous flight control design expertise the following vectors of criteria {P1, P2 , P3, P4 , P5 , P6, FQ1, FQ2, FQ3, FQ4, R1 } and pseudo-criteria {P7, P8, P9, P10, P11, P12, P13} were defined.

### 9.2.4    Criteria Constraints

Based on the metrics defined, the final design of the $\mathfrak{L}_1$ FCS should ideally verify the set of control objectives at the reference flight condition of 80 knots {AU:

Edit OK?} of (equivalent) airspeed and 1,000 ft of altitude. Corresponding to this flight conditions a set of three criteria constraints were defined a priori:

$$P1 \leq 0.1, FQ3 = 1 \text{ and } P4 \leq 1.2$$

The first and second conditions address directly the control specifications, namely, the final value of the step response within 10% of the desired, and the predicted level 1 FQ. The third inequality imposes a 20% constraint on the overshoot in the step response, establishing thus a (loose) bound on the acceptable transient performance characteristics of the actual AOA response. Due to the significant difficulty of defining all criteria constraints consistent with the feasibility of the solution, the rest of the constraints were identified interactively while analyzing the test tables.

## 9.3 Solutions and Analysis

At this point the design optimization task and the nominal prototype solution were completely defined. This section presents last two steps of iterative application of the PSI method to the design improvement of the longitudinal channel of the $\mathscr{L}_1$ FCS. It is critical to mention that the objective of the first iteration is achieved utilizing a limited number of criteria consistent with the control metrics used by the $\mathscr{L}_1$ synthesis procedure. Numerical implementation of this first step is relatively efficient with the "computational price" of one solution measured in minutes. At the second step, while utilizing an extended set of criteria involving complex numerical procedures, the efficiency of numerical implementation becomes critical; the "computational price" of one solution at this step is measured in tenth of minutes.

### 9.3.1 First Iteration

For the purpose of constructing the feasible solution set, we consider the following initial intervals of design variables, which have been defined to include the initial prototype vector (see Table 9.1).

This first step is used to find an initial direction of improvement for the design of the adaptive FCS. More precisely, we aim here at determining tight intervals for the design variables characterizing the state predictor (DV1 and DV2) that would provide level 1 FQ and would not deviate significantly from the desired response defined previously. To this end, the design is to be minimized with respect to the following reduced number of criteria {P1, P2, P3, P4, P5, P6, FQ1, FQ2}, which is a subset of the metrics described earlier.

The robustness metric R1 and the PIO metric FQ4 are not included in this first step because their evaluation is computationally expensive; these

**Table 9.1**
Initial Intervals of Design Variables

| Design Variable | Prototype | Initial Intervals of Variation of Design Variables | |
| --- | --- | --- | --- |
| | | Min | Max |
| DV1 | 5.50E+00 | 4.00E+00 | 8.00E+00 |
| DV2 | 8.50E-01 | 5.00E-01 | 1.10E+00 |
| DV3 | 2.00E+01 | 5.00E+00 | 3.00E+01 |
| DV4 | 2.00E+01 | 1.00E+01 | 5.00E+01 |

metrics will be considered in the next step of the optimization process when the domain of the design variables becomes significantly refined.

The metrics P7 through P10 are not included in the set of criteria to be minimized because improved flying qualities may require "high" values of these metrics. Nevertheless, including these metrics in the optimization process as pseudo-criteria may provide useful information regarding the dynamics of the augmented aircraft. They also provide additional performance characteristics of the set of Pareto optimal solutions. In particular, we note that the metric P9, which is subject to "soft" control specifications, is included as a pseudo-criterion (see [11, 13] for a detailed justification of this choice). Similarly, the metric P11, which can be used to monitor the correct operation of the $\mathfrak{L}_1$ adaptive controller, does not need to be minimized as long as it remains a couple of orders of magnitude below the system state (truncated) $\mathfrak{L}_\infty$ norm. Finally, as explained previously, the metrics P12 and P13 are included for the sake of completeness and should be considered only for the design of the lateral-directional control system. Therefore, they are not included as criteria in the current task.

Next we present the results obtained in this first iteration of the optimization process, which are based on 1,024 tests [11–13]. Out of these 1,024 tests, 427 vectors did not satisfy the a priori given criteria constraints. The solutions that did not satisfy the constraints entered the table of criteria failures [12]. In particular, 160 design variable vectors failed the 20% overshoot criterion constraint on P4, and 267 constraints failed the level 1 FQ criterion constraint FQ3, while the 10% overshoot constraint on P1 was not effective, therefore not rejecting any solutions. Analysis of the design variable vectors contained in the table of criteria failures indicates that: (1) solutions characterized by low natural frequencies and high damping ratios of the state-predictor poles (DV1 < 5 and 0.95 < DV2) fail the level 1 FQ criterion constraint FQ3; and (2) solutions with very high natural frequencies of the state-predictor poles (7.6 < DV1) or solutions with high natural frequencies and low damping ratios of the state-predictor poles (7 < DV1 < 7.6 and DV2 < 0.6) fail the overshoot criterion constraint P4. The first set of design variable vectors leads to slow responses of the

augmented aircraft to pilot commands, which require moderate or considerable pilot compensation and thus result in a predicted level 2 FQ that is inadmissible. The second set corresponds to the solutions providing fast responses to step commands with big overshoots, which differ significantly from the desired response for the augmented aircraft.

The remaining 597 vectors that did satisfy a priori given criteria constraints were used to construct the test table. While tightening the criteria constraints in the test table, the following criteria constraints were formulated (see Table 9.2). Note that while analyzing the test table, the constraint of P4 was significantly tightened to the value of 1.02. It is also worth mentioning that the response on criteria P1 is not presented in the table because all solutions of the test table provided identical response, P1 = 0.

Only 20 solutions were found to be feasible according to these criteria constraints, all of them contributing to the Pareto optimal solutions. A fragment of the criteria table is given in Table 9.3.

Analysis of the criteria table shows that solution #993 is the most preferable one. This solution is equivalent to others with respect to criterion P4; it is superior to others over a set of five criteria {P2, P3, P6, FQ1, FQ2} and is weaker than the prototype only with respect to the criterion P5. Furthermore, the remaining 19 solutions are better than the prototype with respect to four criteria {P2, P3, FQ1, FQ2}. However, none of the solutions are more superior than {AU: Edit OK?} the prototype with respect to criterion P5. In particular, this observation implies that if the prototype design vector was sampled by the system, then it would belong to the Pareto set.

The analysis of the histograms demonstrates the filtering effect of the criteria constraints (see Figure 9.3). The feasible solutions for the design variables DV1 and DV2 are located in the middle of the interval, with no feasible solutions in the left and right ends of the intervals, and slightly shifted from the prototype design (marked with a yellow triangle $\nabla$). These histograms clearly identify feasible intervals for the design variables DV1 and DV2 characterizing

**Table 9.2**
Criteria Constraints

| | | | | |
|---|---|---|---|---|
| P2 $\leq 0.2$ | (min) | P9 $\leq 15$ | (pseudo) |
| P3 $\leq 0.2$ | (min) | P10 $\leq 300$ | (pseudo) |
| P4 $\leq 1.02$ | (min) | P11 $\leq 0.25$ | (pseudo) |
| P5 $\leq 1$ | (min) | P12 $\leq 0.01$ | (pseudo) |
| P6 $\leq 0.3$ | (min) | P13 $\leq 0.01$ | (pseudo) |
| P7 $\leq 0.25$ | (pseudo) | FQ1 $\leq 0.1$ | (min) |
| P8 $\leq 5$ | (pseudo) | FQ2 $\leq 45$ | (min) |

**Table 9.3**
Fragment of Criteria Table

| Criteria | | Prototype | Pareto Optimal Solutions | | | | | | |
| --- | --- | --- | --- | --- | --- | --- | --- | --- | --- |
| | | | #241 | #281 | #329 | #409 | #649 | #825 | #993 |
| P2 | (min) | 1.30E-01 | 1.04E-01 | 8.40E-02 | 9.14E-02 | 8.97E-02 | 6.03E-02 | 7.44E-02 | 5.39E-02 |
| P3 | (min) | 1.54E-01 | 1.16E-01 | 1.03E-01 | 1.06E-01 | 1.04E-01 | 8.72E-02 | 9.51E-02 | 8.84E-02 |
| P4 | (min) | 1.0E+00 | 1.00E+00 | 1.00E+00 | 1.00E+00 | 1.00E+00 | 1.01E+00 | 1.00E+00 | 1.00E+00 |
| P5 | (min) | 3.15E-01 | 5.37E-01 | 9.36E-01 | 9.68E-01 | 6.29E-01 | 8.63E-01 | 8.58E-01 | 6.89E-01 |
| P6 | (min) | 1.49E-01 | 1.97E-01 | 2.21E-01 | 2.58E-01 | 2.03E-01 | 1.74E-01 | 1.94E-01 | 1.32E-01 |
| P7 | (pseudo) | 1.51E-01 | 1.65E-01 | 1.74E-01 | 1.84E-01 | 1.72E-01 | 1.83E-01 | 1.78E-01 | 1.75E-01 |
| P8 | (pseudo) | 3.24E+00 | 3.3E+00 | 3.29E+00 | 3.31E+00 | 3.30E+00 | 3.31E+00 | 3.30E+00 | 3.31E+00 |
| P9 | (pseudo) | 5.96E+00 | 1.17E+01 | 7.55E+00 | 9.1E+00 | 1.09E+01 | 1.11E+01 | 9.36E+00 | 1.16E+01 |
| P10 | (pseudo) | 1.07E+02 | 2.42E+02 | 1.34E+02 | 1.72E+02 | 2.16E+02 | 2.24E+02 | 1.76E+02 | 2.44E+02 |
| P11 | (pseudo) | 7.45E-02 | 7.79E-02 | 6.02E-02 | 6.82E-02 | 8.10E-02 | 7.72E-02 | 7.22E-02 | 7.77E-02 |
| P12 | (pseudo) | 1.01E-04 | 1.84E-04 | 1.87E-04 | 2.08E-04 | 2.06E-04 | 2.29E-04 | 2.14E-04 | 2.09E-04 |
| P13 | (pseudo) | 3.16E-05 | 6.18E-05 | 6.87E-05 | 8.01E-05 | 7.00E-05 | 8.18E-05 | 7.58E-05 | 7.03E-05 |
| FQ1 | (min) | 1.23E-02 | 6.73E-02 | 9.29E-02 | 9.74E-02 | 6.86E-02 | 9.05E-02 | 7.80E-02 | 8.85E-02 |
| FQ2 | (min) | 5.36E+01 | 4.42E+01 | 4.35E+01 | 4.03E+01 | 4.22E+01 | 3.79E+01 | 4.10E+01 | 4.00E+01 |

the state-predictor dynamics. On the other hand, the feasible solutions for the design variables DV3 and DV4 are located at the right boundaries of the intervals. These observations will be used in the next step of the optimization process to modify the initial intervals in the direction of higher density of feasible solutions to improve richness of the feasible solution set.

It is also important to analyze the influence of the design variables on criteria and pseudo-criteria and to evaluate the degree of improvement (or
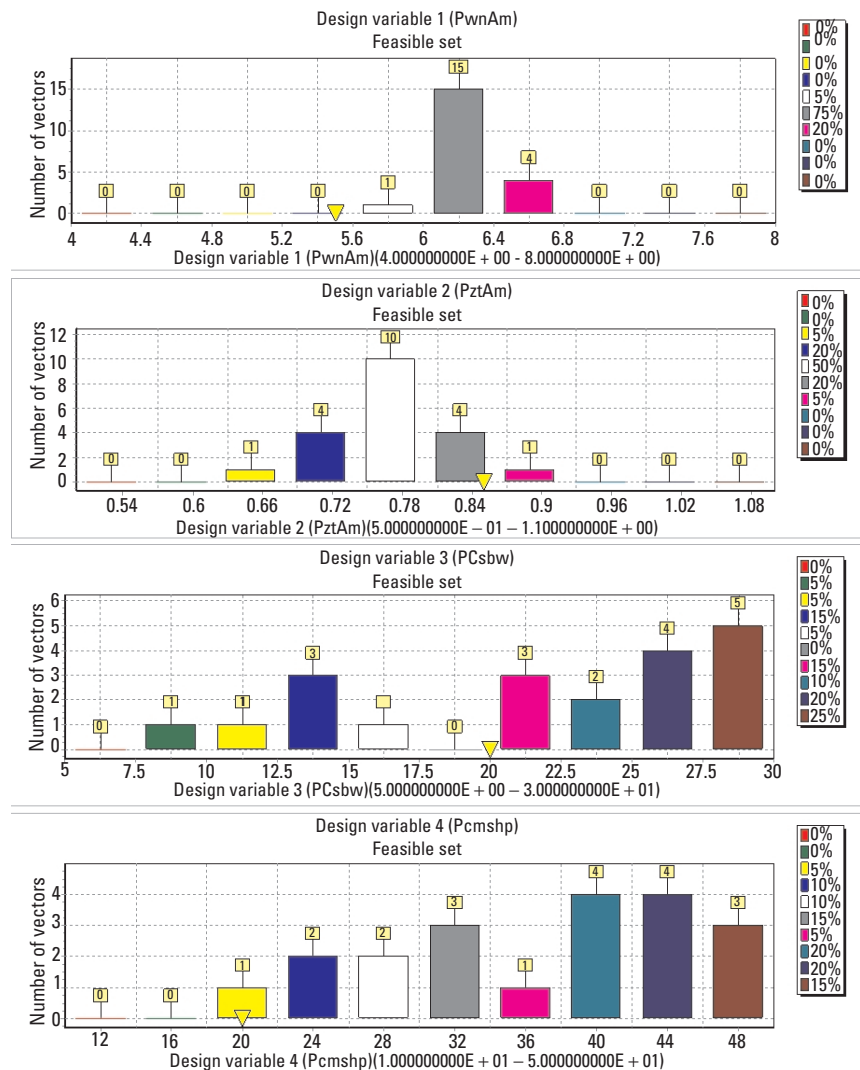


**Figure 9.3** PSI iteration 1, distribution of feasible solutions; yellow triangle shows the prototype design.

degradation) of the Pareto optimal solutions with respect to the prototype design. Figures 9.4 to 9.8 show some of these dependencies, which provide valuable insight into the effect of the design variables on the augmented aircraft dynamics. Preliminary conclusions that can be drawn from this analysis are detailed next.

Figure 9.4 shows a typical dependency of criteria P2 (P3 and P6 have the same trend) on the design variable DV1. First, we notice that there are no feasible solutions in the range $4 < DV1 < 4.6$, which indicates that such design variable vectors did not satisfy the constraints. Second, it can be seen that the deviations of the actual response (P2, P3, and P6) of the augmented aircraft from the desired model become large for big values of the design variable DV1. Third, all three dependencies show that the set of Pareto optimal solutions, when compared to the prototype design, provide step responses with reduced deviations in terms of both (truncated) $\mathcal{L}_\infty$ and $\mathcal{L}_2$ norms. The rate deviations for the Pareto optimal solutions are, however, larger than the rate deviations for the prototype design.

Figure 9.5 presents the dependencies of the flying qualities criteria FQ2 (FQ1 has the same trend) on the design variable DV1, which indicate that faster responses of the augmented aircraft (large DV1) result in improved (predicted) flying qualities. This trend is particularly evident in Figure 9.5, in which the reduced pilot (lead) compensation is limited to large values of the design variable DV1. Also, when compared to the prototype design, the set of optimal solutions improve the criterion FQ1 by 20% to 50%, and the criterion FQ2 by 15% to 30%.

As expected, a faster response of the augmented aircraft (large DV1) leads to an increase in the control effort (pseudo-criteria P8), as well as an increase in both the maximum elevator rate and the maximum elevator acceleration (pseudo-criteria P9 and P10).
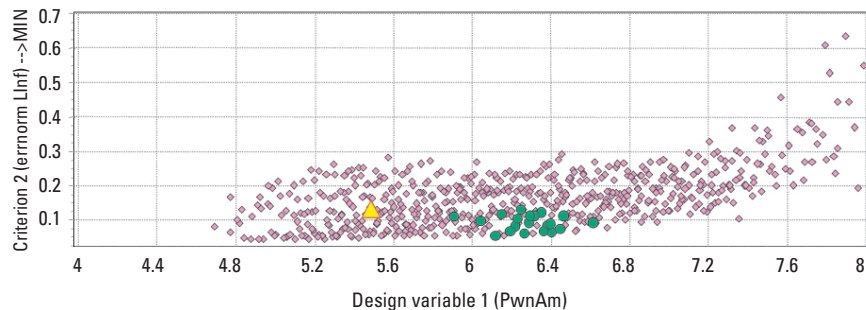


**Figure 9.4** PSI iteration 1; dependencies of the criterion P2 (maximum AOA deviation) on the design variable DV1.
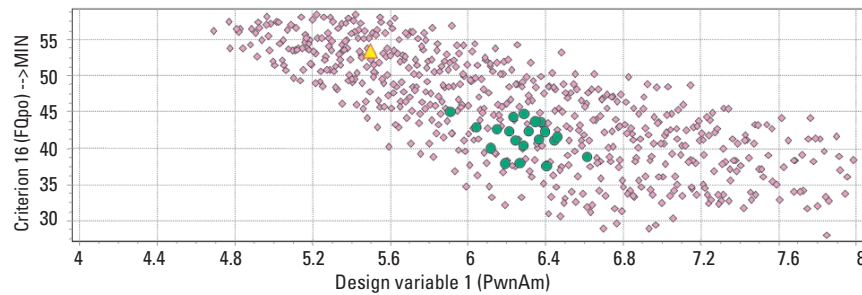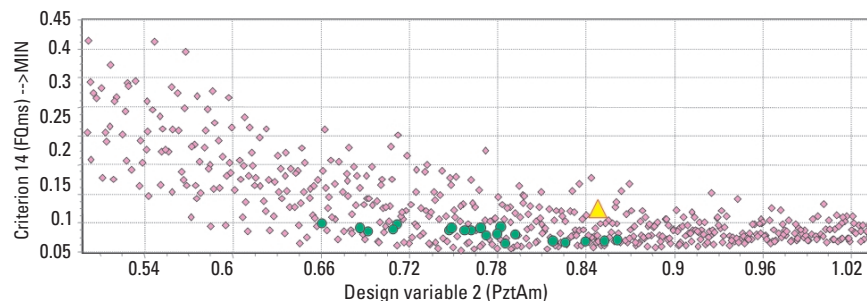
**Figure 9.5** PSI iteration 1; dependencies of the criterion FQ2 (pilot workload) on the design variable DV1.

Figure 9.6 illustrates the dependencies of criteria FQ1 on the design variable DV2. (FQ2 has the same trend.) While the dependency of FQ2 on DV2 is not obvious, small values of DV2 seem to limit the achievable tracking performance with the pilot in the loop (FQ1). This would imply that the augmented aircraft with low-damping characteristics result in degraded (predicted) flying qualities.

Finally, the dependencies of pseudo-criteria P9 and P10 on the design variable DV4 show that the Pareto optimal solutions are located along a "straight" line with positive slope where high values of the criteria correspond to high values of the design variable DV4. This implies that the bandwidth of the command prefilter in the $\mathcal{L}_1$ FCS (DV4) can be set to limit the maximum elevator rate and the maximum elevator acceleration of the Pareto optimal solutions.

Dependencies between criteria provide useful information about the solutions in the Pareto set and the trade-offs between criteria. The analysis of trade-offs becomes especially helpful in the final stages of the optimization process, when a decision about the most preferable solution has to be made. These
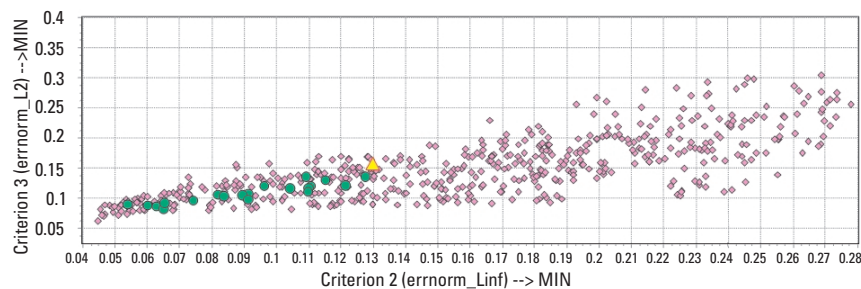


**Figure 9.6** PSI iteration 1; dependencies of the criteria {AU: Should this be singular?} FQ1 (tracking performance) on the design variable DV2.

dependencies are useful to explore the trade-offs in the design of the controller and to identify directions in the design variable space that may lead to improved $\mathfrak{L}_1$ FCS design over the prototype design.

Next we present and discuss a set of results showing dependencies between criteria illustrating these trade-offs and determining possible directions of improvement of the prototype solution:

Figure 9.7 shows the dependency between P2 and P3 (maximum and integral deviations from the desired response) as well as the localization of the Pareto optimal solutions with respect to the prototype design in the P2-P3 plane. It can be seen that the solutions of the Pareto set are located on a "straight" line passing through the prototype design, and all of them improve the prototype in terms of the metrics P2 and P3.

Figure 9.8 shows the location of the prototype as well as the Pareto optimal solutions in the FQ plane of the TDNS criteria, thus characterizing the (predicted) flying qualities of the solutions. The improvement with respect to the prototype design in terms of predicted FQ is evident in this FQ2-FQ1



**Figure 9.7**  PSI iteration 1; dependencies between criteria P2 and P3 (maximum and integral deviation of AOA).
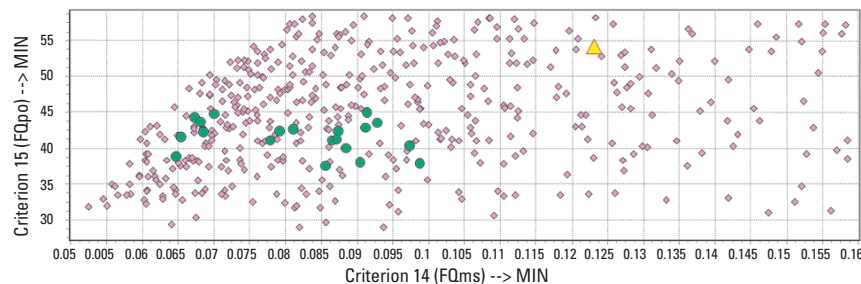


**Figure 9.8**  PSI iteration 1; dependencies between criteria FQ1 and FQ2 (tracking performance and pilot workload).

graph. Also, the boundary for level 1 FQ of the TDNS criterion can be easily recognized in this figure (see [16]).

Finally, Figure 9.9 shows the dependency between the FQ criterion FQ2 and the control effort P8. This figure shows that reduced pilot (lead) compensation is only possible for increased control effort. In fact, all of the solutions in the Pareto set present higher control efforts than the prototype solution.

The analysis of the obtained solutions allows us to define the direction of further search. In particular, the results have provided tight intervals for the design variables DV1 and DV2 characterizing the state-predictor dynamics, and have exposed the necessity of extending the initial intervals of initial intervals of variation of the design variables DV3 and DV4. It is worth emphasizing that this significant improvement of the prototype solution has been achieved utilizing a reduced number of criteria, {P2, P3, P4, P5, P6, FQ1, FQ2}. Based on these results and the conclusions drawn from them, a new experiment is carried out to: (1) improve the feasible solution set, and (2) determine an optimal solution of the $\mathfrak{L}_1$ FCS design that improves the prototype with respect to extended set of criteria {P2, P3, P4, P5, P6, FQ1, FQ2, FQ4, R1}.

### 9.3.2   Second Iteration

The improvement of the feasible solution set is based on the analysis of the histograms in Figure 9.3 and Table 9.3. The analysis of the histograms results in adjusting the initial problem statement by changing the intervals of variation of the design variables is given in Table 9.4.

The criteria constraints remain unchanged, whereas the design is now to be optimized with respect to the following new set of criteria {P2, P3, P4, P5, P6, FQ1, FQ2, FQ4, R1}. All these criteria are to be minimized except for R1, which is to be maximized.

Next we present the results obtained in this second iteration of the optimization process, which are based on 512 tests. As mentioned previously, adding
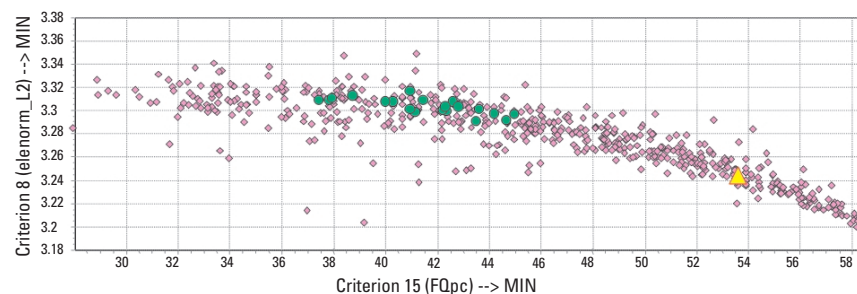


**Figure 9.9**  PSI iteration 1, dependencies between criteria FQ2 and P8 (pilot workload and maximum AOA deviation).

**Table 9.4**
Refined Intervals of Design Variables

| Design Variable | Prototype | Initial Intervals of Variation of Design Variables | |
|---|---|---|---|
| | | Min | Max |
| DV1 | 5.50E+00 | 5.50E+00 | 7.00E+00 |
| DV2 | 8.50E-01 | 6.50E-01 | 0.90E+00 |
| DV3 | 2.00E+01 | 9.80E+00 | 4.00E+01 |
| DV4 | 2.00E+01 | 1.80E+01 | 6.50E+01 |

criteria R1 and FQ4 in the optimization process represents a significant increase in the computational time. Approximately 124 vectors satisfied previously assigned criteria constraints (see Table 9.2). All these solutions are Pareto optimal. As might be expected, the coefficient of selection efficiency γ increased by more than 12 times. The histograms in the second iteration have better distributions (higher concentration) of the feasible solutions than in the first iteration. The top of Figure 9.10 represents the distribution of 124 solutions for DV1.

After the analysis of the test table, stronger criteria and pseudo-criteria constraints were considered as presented in Table 9.5. According to these new constraints, only six solutions were found to be feasible, and all of them are
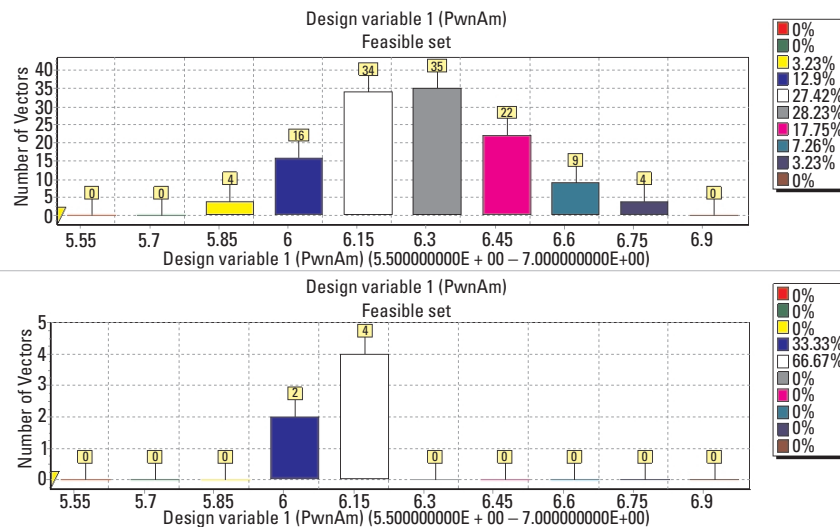


**Figure 9.10** PSI iteration 2, distribution of feasible solutions of DV1 with the original (top) and with tightened criteria constraints (bottom).

**Table 9.5**

Second Iteration, Refined Criteria Constraints

| | | | |
|---|---|---|---|
| $P2 \leq 0.1$ | (min) | $P10 \leq 200$ | (pseudo) |
| $P3 \leq 0.15$ | (min) | $P11 \leq 0.1$ | (pseudo) |
| $P4 \leq 1.02$ | (min) | $P12 \leq 0.01$ | (pseudo) |
| $P5 \leq 1$ | (min) | $P13 \leq 0.01$ | (pseudo) |
| $P6 \leq 0.25$ | (min) | $FQ1 \leq 0.1$ | (min) |
| $P7 \leq 0.2$ | (pseudo) | $FQ2 \leq 45$ | (min) |
| $P8 \leq 5$ | (pseudo) | $FQ4 \leq 5$ | (min) |
| $P9 \leq 10$ | (pseudo) | $R1 \geq 80$ | (max) |

Pareto optimal. The values of design variables and criteria of the Pareto optimal solutions are given in Table 9.6. The new distribution of the feasible solutions for these criteria and pseudo-criteria constraints is significantly tighter as expected and is shown in the bottom of Figure 9.10. These new histograms clearly identify tight intervals for all of the design variables in which the optimal solutions lie.

Furthermore, from the analysis of Table 9.6, it follows that all solutions of second iteration as well as the #993 from the first iteration belong to the very tight intervals of the first and second design variables. The first three parameters (DV1–DV3) of #993 and #106 are almost identical. Observe that #993, while providing good response of many criteria, does not satisfy new constraints on criteria P9 and P10 (the elevator workload). Moreover, the analysis of the #993 also shows that it fails to satisfy constraint of the flying qualities criteria FQ3.

The analysis of test tables, dependencies of criteria on design variables, and dependencies between criteria allows us to determine the most preferable solutions.

In particular, Figure 9.11 shows the influence of the bandwidth of the "matched" lowpass filter (DV3) on the (pilot-off-the-loop) trade-off between performance criterion P2 (P3 shows the same trend) and robustness (R1) of the augmented aircraft. From this observation we can conclude that criteria P2 (P3) and R1 are contradictory with respect to the design variable DV3. This means that improvement of the tracking performance requires an increase in the bandwidth of the lowpass filter, which in turn results in degradation of the time delay margin of the augmented aircraft, as predicted by theory.

Figure 9.12 shows the dependencies of the flying qualities criterion FQ1 (FQ2 shows a similar trend) on the design variable DV2. While in the first PSI iteration the dependency of the criterion FQ2 on the design variable DV2 was not obvious, now it becomes more apparent that a smaller damping ratio seems to result in reduced (lead) pilot compensation.
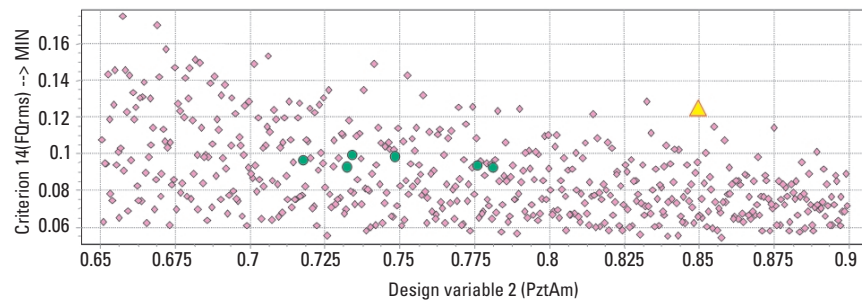
**Table 9.6**
Second Iteration: Table of Design Variables

| Design variable | Prototype | #993, First Iteration | Pareto Optimal Solutions | | | | | |
|---|---|---|---|---|---|---|---|---|
| | | | #106 | #202 | #254 | #318 | #358 | #462 |
| DV1 | 5.50E+00 | 6.12E+00 | 6.00E+00 | 5.99E+00 | 6.24E+00 | 6.23E+00 | 6.10E+00 | 6.18E+00 |
| DV2 | 8.50E+00 | 7.09E-01 | 7.34E-01 | 7.49E-01 | 7.76E-01 | 7.33E-01 | 7.81E-01 | 7.18E-01 |
| DV3 | 2.0E+01 | 2.70E+01 | 2.52E+01 | 1.67E+01 | 1.81E+01 | 2.18E+01 | 1.69E+01 | 1.58E+01 |
| DV4 | 2.0E+01 | 4.93E+01 | 3.16E+01 | 3.20E+01 | 2.10E+01 | 2.72E+01 | 2.57E+01 | 3.11E+01 |
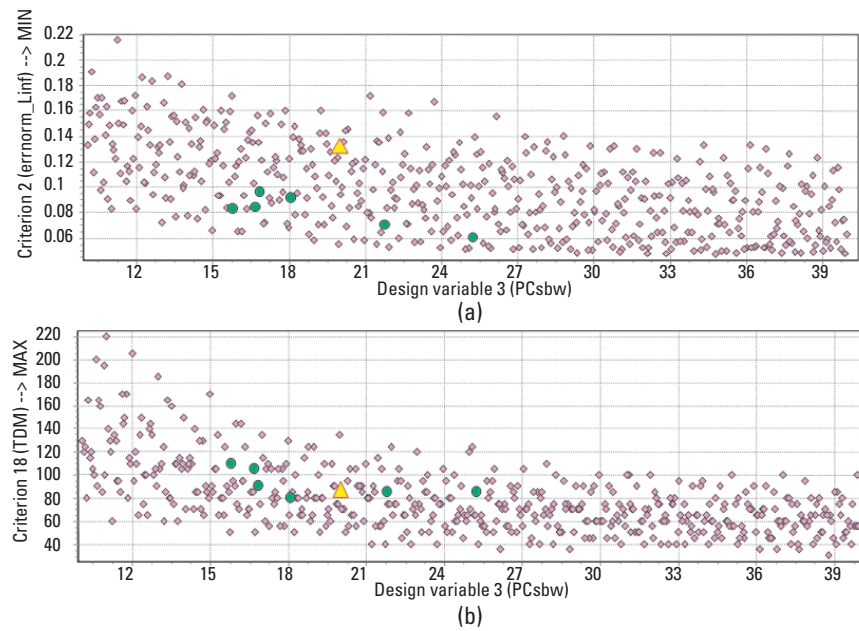
**Figure 9.11** PSI iteration 2, dependencies of criteria P2 and R1 on the design variable DV3.



**Figure 9.12** PSI iteration 2, dependencies of criteria FQ1 (tracking performance) on the design variable DV2.

Dependency between P2 and P3 is analogous to those obtained in first iteration; therefore, the corresponding figure is not presented. All of the Pareto optimal solutions improve the prototype design in terms of peak and integral deviations from the desired response.

The dependency of flying qualities criteria FQ1 and FQ2 obtained in this iteration is also similar to those obtained in the first iteration, thus

**Table 9.7**

Second Iteration: Table of Criteria

| Criteria | | Prototype | Pareto Optimal Solutions | | | | | |
|---|---|---|---|---|---|---|---|---|
| | | | #106 | #202 | #254 | #318 | #358 | #462 |
| P2 | (min) | 1.30E-001 | 6.01E-01 | 8.45E-02 | 9.17E-02 | 7.04E-02 | 9.63E-02 | 8.28E-02 |
| P3 | (min) | 1.54E-01 | 9.60E-02 | 1.13E-01 | 1.11E-01 | 9.66E-02 | 1.18E-01 | 1.04E-01 |
| P4 | (min) | 1.0E+00 | 1.00E+00 | 1.00E+00 | 1.00E+00 | 1.00E+00 | 1.01E+00 | 1.00E+00 |
| P5 | (min) | 3.15E-01 | 6.13E-01 | 6.81E-01 | 8.85E-01 | 8.43E-01 | 7.71E-01 | 8.63E-01 |
| P6 | (min) | 1.49E-01 | 1.28E-01 | 1.67E-01 | 2.16E-01 | 1.78E-01 | 1.94E-01 | 2.11E-01 |
| P7 | (pseudo) | 1.51E-01 | 1.68E-01 | 1.67E-01 | 1.72E-01 | 1.76E-01 | 1.68E-01 | 1.78E-01 |
| P8 | (pseudo) | 3.24E+00 | 3.29E+00 | 3.29E+00 | 3.29E+00 | 3.30E+00 | 3.29E+00 | 3.31E+00 |
| P9 | (pseudo) | 5.96E+00 | 9.09E+00 | 9.1E+00 | 7.9E+00 | 9.05E+00 | 8.43E+00 | 9.54E+00 |
| P10 | (pseudo) | 1.07E+02 | 1.77E+02 | 1.78E+02 | 1.43E+02 | 1.72E+02 | 1.59E+02 | 1.85E+02 |
| P11 | (pseudo) | 7.45E-02 | 6.62E-02 | 6.60E-02 | 6.09E-02 | 6.74E-02 | 6.31E-02 | 6.95E-02 |
| P12 | (pseudo) | 1.01E-04 | 1.81E-04 | 1.70E-04 | 1.80E-04 | 2.01E-04 | 1.69E-04 | 1.98E-04 |
| P13 | (pseudo) | 3.16E-05 | 6.02E-05 | 5.89E-05 | 6.58E-05 | 7.13E-05 | 6.01E-05 | 7.27E-05 |
| FQ1 | (min) | 1.23E-02 | 9.93E-02 | 9.81E-02 | 9.34E-02 | 9.26E-02 | 9.20E-02 | 9.64E-02 |
| FQ2 | (min) | 5.36E+01 | 4.33E+01 | 4.41E+01 | 4.38E+01 | 4.14E+01 | 4.46E+01 | 4.10E+01 |
| FQ4 | (min) | 4.68E+00 | 4.08E+00 | 4.19E+00 | 3.87E+00 | 3.88E+00 | 3.84E+00 | 3.97E+00 |
| R1 | (max) | 8.50E+01 | 8.50E+01 | 1.05E+02 | 8.00E+01 | 8.50E+01 | 9.00E+01 | 1.00E+02 |

demonstrating significant improvement of predicted flying qualities over the prototype design but now in the extended criteria space.

Finally, Figure 9.13 shows the dependency between criteria P3 and R1, which illustrates the trade-off between performance and robustness of the closed-loop adaptive system with the pilot off the loop. While all of the optimal solutions reduce the deviations from the desired response with respect to the prototype design, only three of these solutions exhibit a better time-delay margin than the prototype design (#202, #462), and two exhibit a similar margin (#106, #318)[3].

As a result of the iterative two-step correction of initial constraints, the six Pareto optimal solutions have been found. Analyzing the criteria table shows that there are no solutions better than the prototype by all criteria simultaneously. This analysis revealed that four solutions, #106, #202, #358, and #462, surpassed the prototype by six criteria simultaneously.

Although all six solutions are practically equivalent, some advantage is given to the design vector #202 since it provides a better trade-off between the (predicted) flying qualities (FQ1, FQ2) and the time-delay margin (R1), while minimizing the difference with the desired response (see Figure 9.14). The comparative analysis of the AOA and the elevator workload demonstrates that the optimal solution provides faster response (rise time) to the commanded AOA command while minimally increasing the elevator workload that is naturally expected.
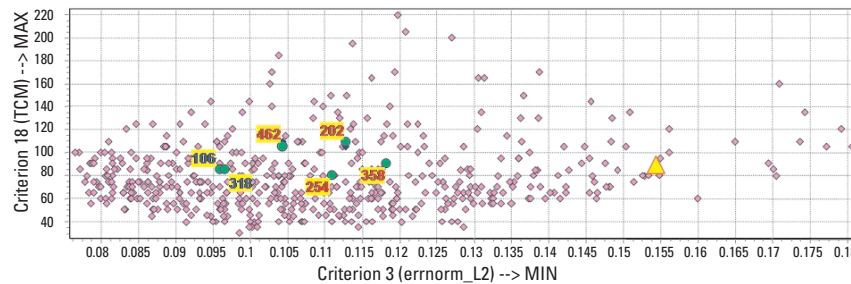


**Figure 9.13** PSI iteration 2; dependencies between criteria R1 (time delay margin) and P3 (integral deviation of AOA).

---

3. Notice that for the determination of the time-delay margin, metric R1, we insert incremental time delays of 5 ms in the elevator command channel. This choice was made for consistency with the determination of the time-delay margin in the AirSTAR real-time simulator at NASA LARC. As a consequence, however, we cannot identify the time-delay margin with higher accuracy.
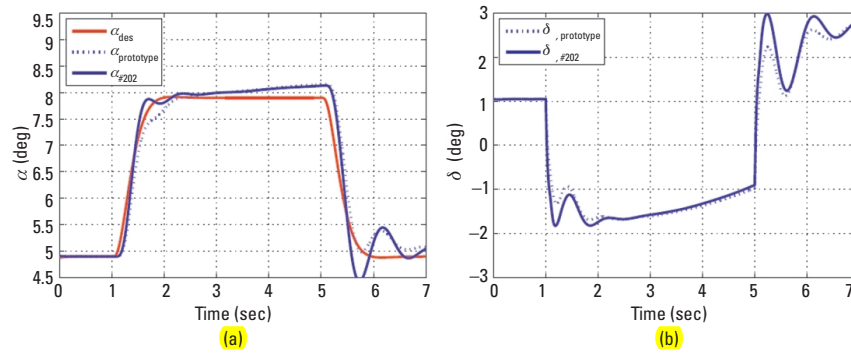
**Figure 9.14** Optimal design #202, 3° AOA step response.

### 9.3.3   Conclusion

The construction of the feasible solutions of the $\mathcal{L}_1$ adaptive controller satisfying the desired performance and robustness specifications is a critical step for the optimal design of the $\mathcal{L}_1$ FCS. In particular, the eigenstructure of the state-predictor state matrix and the bandwidth of the lowpass filters are the key elements that characterize the performance of the $\mathcal{L}_1$ FCS. To optimize the design of these elements, an 18-criteria problem of improving a prototype solution was formulated and solved. The results presented demonstrate the application of PSI method to the multicriteria design optimization of the $\mathcal{L}_1$ FCS implemented on the GTM AirSTAR aircraft. The study has addressed both the construction of the feasible solution set and the improvement of a nominal prototype design initially synthesized by the $\mathcal{L}_1$ theory.

On one hand, the results have demonstrated that the consistent application of the systematic design guidelines of $\mathcal{L}_1$ adaptive control becomes particularly beneficial for the construction of the feasible solution set. Moreover, the results of this study are consistent with the theoretical claims of the theory of $\mathcal{L}_1$ adaptive control in terms of robustness and performance. On the other hand, the developed procedure and the obtained results confirm the suitability of the PSI method and the MOVI software package for the multicriteria optimization of an adaptive FCS subject to desired control specifications.

The optimal design of the $\mathcal{L}_1$ FCS significantly improved understanding of the design trade-offs between adaptation and robustness. Finally, the design guidelines learned during the interaction with GTM model utilizing MOVI software contributed to the successful flight verification and validation of the designed all-adaptive control law at NASA LARC.

# References

[1] Jacklin, S. A., et al., "Verification, Validation, and Certification Challenges for Adaptive Flight-Critical Control System Software," AIAA Guidance, Navigation and Control Conference, AIAA-2004-5258, Providence, RI, August 2004.

[2] Wise, K. A., E. Lavretsky, and N. Hovakimyan, "Adaptive Control in Flight: Theory, Application, and Open Problems," American Control Conference, Minneapolis, MN, June 2006, pp. 5966–5971.

[3] Jacklin, S. A., "Closing Certification Gaps in Adaptive Flight Control Software," AIAA Guidance, Navigation and Control Conference, AIAA-2008-6988, Honolulu, HI, August 2008.

[4] Hovakimyan, N., and C. Cao, $\mathcal{L}_1$ Adaptive Control Theory, Philadelphia, PA: Society for Industrial and Applied Mathematics, 2010.

[5] Jordan, T. L., W. M. Langford, and J. S. Hill, "Airborne Subscale Transport Aircraft Research Testbed-Aircraft Model Development," AIAA Guidance, Navigation and Control Conference, AIAA-2005-6432, San Francisco, CA, August 2005.

[6] Jordan, T. L., et al., "AirSTAR: A UAV Platform for Flight Dynamics and Control System Testing," AIAA Aerodynamic Measurement Technology and Ground Testing Conference, AIAA-2006-3307, San Francisco, CA, June 2006.

[7] Xargay, E., N. Hovakimyan, and C. Cao, "$\mathcal{L}_1$ Adaptive Controller for Multi-Input Multi-Output Systems in the Presence of Nonlinear Unmatched Uncertainties," American Control Conference, Baltimore, MD, June–July 2010.

[8] Gregory, I. M., et al., "$\mathcal{L}_1$ Adaptive Control Design for NASA AirSTAR Flight Test Vehicle," AIAA Guidance, Navigation and Control Conference, AIAA-2009-5738, Chicago, IL, August 2009.

[9] Gregory, I. M., et al., "Flight Test of an $\mathcal{L}_1$ Adaptive Controller on the NASA AirSTAR Flight Test Vehicle," AIAA Guidance, Navigation and Control Conference, Toronto, Canada, August 2010.

[10] Kim, K. K., and N. Hovakimyan, "Development of Verification and Validation Approaches for $\mathcal{L}_1$ Adaptive Control: Multi-Criteria Optimization for Filter Design," AIAA Guidance, Navigation and Control Conference, Toronto, Canada, August 2010.

[11] Statnikov, R. B., and J. B. Matusov, Multicriteria Analysis in Engineering, Dordrecht/Boston/London: Kluwer Academic Publishers, 2002.

[12] Yanushkevich, I. V., et al., Software Package MOVI 1.3 for Windows: User's Manual, United States Copyright Office, the Library of Congress, 2004.

[13] Sobol, I. M., and R. B. Statnikov, Selecting Optimal Parameters in Multicriteria Problems, 2nd ed., (in Russian), Moscow: Drofa, 2006.

[14] Xargay, E., et al., "$\mathcal{L}_1$ Adaptive Flight Control System: Systematic Design and V&V of Control Metrics," AIAA Guidance, Navigation, and Control Conference, Toronto, Ontario, Canada, August 2–5, 2010.

[15]   Stepanyan, V., et al., "Stability and Performance Metrics for Adaptive Flight Control,"
       AIAA Guidance, Navigation and Control Conference, Chicago, IL, AIAA-2009-5965,
       August 2009.

[16]   Bailey, R. E. and T. J. Bidlack, Unified Pilot-Induced Oscillation Theory, Volume IV:
       Time-Domain Neal-Smith Criterion, Tech. Rep. WL-TR-96-3031, Air Force Wright
       Laboratory, December 1995.

[17]   Choe, R., et al., "$\mathcal{L}_1$ Adaptive Control Under Anomaly: Flying Qualities and Adverse Pilot
       Interaction," AIAA Guidance, Navigation and Control Conference, Toronto, Canada,
       August 2010.